Journal of Materials Chemistry

Cite this: *J. Mater. Chem.*, 2011, **21**, 18630

www.rsc.org/materials

PAPER

Sol–gel synthesis and electrochemical properties of fluorophosphates $Na_2Fe_{1-x}Mn_xPO_4F/C$ ($x = 0, 0.1, 0.3, 0.7, 1$) composite as cathode materials for lithium ion battery

Xiaobiao Wu,[a] Jianming Zheng,[a] Zhengliang Gong[b] and Yong Yang*[ab]

Received 27th July 2011, Accepted 14th September 2011
DOI: 10.1039/c1jm13578c

Fluorophosphates $Na_2Fe_{1-x}Mn_xPO_4F/C$ ($x = 0, 0.1, 0.3, 0.7, 1$) composite were successfully synthesized *via* a sol–gel method. The structure, morphology and electrochemical performance of the as prepared materials were studied by X-ray diffraction (XRD), scanning electron microscopy (SEM), transmission electron microscopy (TEM) and charge/discharge measurements. XRD results show that, consistent with Na_2FePO_4F, $Na_2Fe_{0.9}Mn_{0.1}PO_4F$ ($x = 0.1$) crystallize in a two-dimensional (2D) layered structure with space group *Pbcn*. However, increasing the content of Mn to $x \geq 0.3$ results in a structure transition of $Na_2Fe_{1-x}Mn_xPO_4F$ from the 2D layered structure of Na_2FePO_4F to the three-dimensional (3D) tunnel structure of Na_2MnPO_4F. SEM and TEM analysis indicates nanostructured primary particles (about tens of nanometres in diameter) are obtained for all samples due to uniform carbon distribution and low calcining temperature used. Na_2FePO_4F is able to deliver a reversible capacity of up to 182 mA h g^{-1} (about 1.46 electrons exchanged per unit formula) with good cycling stability. Compared with Na_2FePO_4F, partial replacement of Fe by Mn in $Na_2Fe_{1-x}Mn_xPO_4F$ increases the discharge voltage plateau. Similar to Na_2FePO_4F, iron-manganese mixed solid solution $Na_2Fe_{1-x}Mn_xPO_4F$ ($x = 0.1, 0.3, 0.7$) also show good cycling performance. Furthermore, Na_2MnPO_4F with high electrochemical activity was successfully prepared for the first time, which is able to deliver a discharge capacity of 98 mA h g^{-1}. The good electrochemical performance of $Na_2Fe_{1-x}Mn_xPO_4F$ materials can be attributed to the distinctive improvement of ionic/electronic conduction of the materials by formation of nanostructure composite with carbon.

1. Introduction

Lithium-ion batteries have been widely used in laptops, cell phones and electric vehicles because of their excellent performance. However, cathode materials used in present Li-ion battery systems have restricted further enhancement in energy density of lithium-ion batteries.[1] For example, $LiCoO_2$ suffers from high cost, toxicity, and structural instability at deep charge which is considered not suitable for batteries used in hybrid electric vehicle (HEV) and electric vehicle (EV). $LiFePO_4$ as one kind of polyanion cathodes introduced by Goodenough *et al.* in 1997 is inexpensive, environmentally friendly and stable both chemically and thermally.[2] Since then, polyanion based cathode materials have attracted great interest and a lot of new polyanion compounds were developed and investigated.[3,4] In order to achieve higher energy density, cathode materials with higher voltage plateau and higher capacity have attracted wide attention in recent years.[1] Fluorides have higher electronegativity compared with oxides, which increases the ionicity of the bonds and their redox potentials.[1,5] Besides, the addition of fluorine atom brings in a negative charge, so another positive charge is needed in order to maintain charge balance, which may result in higher capacity.

As introduced by Ramesh *et al.*,[6] $LiFePO_4F$ has a voltage plateau of 3.0 V higher than isotypic compound $LiFePO_4OH$ (2.6 V). However, the voltage plateau of $LiFePO_4F$ is lower than that of $LiFePO_4$ (3.4 V), mainly due to their different structures. If we need to increase the energy density of the material, we need to explore the utilization of the two electron redox process of $Fe^{2+/3+}$ and $Fe^{3+/4+}$. In another report, Recham *et al.* used Mössbauer measurements to confirm that Fe^{4+} can be observed when $LiFePO_4F$ is charged to higher voltage (4.2 V), but no more than one electron can be reversibly cycled in their experimental condition.[7]

In 2007, Ellis *et al.*[8] used solid-state reaction and sol–gel process to synthesize a new class of sodium-based fluorophosphate: Na_2FePO_4F. Na_2FePO_4F has a two-dimensional (2D) layered structure, which makes its electronic conductivity higher than that of $LiFePO_4$. As there are two sodium ions in

[a]*State Key Laboratory for Physical Chemistry of Solid Surfaces, and Department of Chemistry, College of Chemistry and Chemical Engineering, Xiamen University, Xiamen, 361005, PR China. E-mail: yyang@xmu.edu.cn; Tel: +86-592-218-5753*
[b]*School of Energy Research, Xiamen University, Xiamen, 361005, China*

Na_2FePO_4F, exchange of more than one electron may occur during charge/discharge. Unfortunately, only 0.8 electron exchange per unit formula can be achieved. In following Recham's study,[9] Na_2FePO_4F was prepared by the ionothermal approach, and the performance of the materials was improved, and it delivered 120 mA h g^{-1} (about one electron exchange per unit formula).

Since Mn-based phosphates normally have higher redox potential than Fe-based phosphates,[10] it should be possible for Na_2MnPO_4F to achieve higher potential than Na_2FePO_4F. Different to 2D layered Na_2FePO_4F, Na_2MnPO_4F has a three-dimensional (3D) tunnel structure with space group $P2_1/n$.[11] Na_2MnPO_4F prepared by solid-state reaction or ionothermal process were all found to be electrochemically inactive despite an open pathway for alkali migration even being charged up to 5 V.[9,12] At the same time, it was also found that there was no reaction observed upon mixing the material with NO_2BF_4. Whether this is due to the structural distinction of Na_2MnPO_4F is not clear at present. In their work, Ellis *et al.* supposed that decreasing the particle size through proper methods may help to achieve the electrochemical activity of Na_2MnPO_4F.[12] Recham *et al.* also repeated the same system with an ionothermal method and suggested that the structure difference of Na_2FePO_4F and Na_2MnPO_4F can be attributed to the difference in ionic radii between Fe^{2+} and Mn^{2+}. The bigger radius of Mn (83 pm) than Fe (78 pm) results in a three-dimensional tunnel structure of Na_2MnPO_4F compared to a two-dimensional layered structure of Na_2FePO_4F.[9] For Na_2FePO_4F, two FeO_4F_2 octahedra share faces, but for Na_2MnPO_4F, in order to minimize the repulsive interactions, two MnO_4F_2 octahedra turn to share corners. The structure and electrochemical performance of $Na_2Fe_{1-x}Mn_xPO_4F$ series were also studied. As the Mn content increases to 0.25, $Na_2Fe_{1-x}Mn_xPO_4F$ changes from a 2D layered structure to a 3D tunnel structure just as with Na_2MnPO_4F, which also show electrochemical activity indicating that this structure has open pathways for ion migration, even though its electrochemical performance is poorer and voltage plateau is lower compared with 2D layered Na_2FePO_4F. However, it seems that the substitution of Fe by Mn shows no effect on the redox potential of $Na_2Fe_{1-x}Mn_xPO_4F$ in that work. The authors can't conclude whether these results are due to the poor electronic–ionic conductivity of Mn-based fluorophosphates or the open pathways in 3D tunnel structure of $Na_2Fe_{1-x}Mn_xPO_4F$ being unfavorable for Li^+/Na^+ intercalation/deintercalation. Therefore, it should be very interesting to consider the following questions: Can Na_2FePO_4F achieve exchange of more than one electron? Can Na_2MnPO_4F show any electrochemical activity? The positive answers to above questions should be beneficial to further explore such fluorine-substituted polyanion systems.

In this investigation, a novel sol–gel process is proposed to prepare nanostructured $Na_2Fe_{1-x}Mn_xPO_4F/C$ ($x = 0$, 0.1, 0.3, 0.7, 1) composite cathode materials. We have investigated systematically the structure, morphology and electrochemical activity of Na_2FePO_4F and Na_2MnPO_4F. We also compared the structures and electrochemical performance of $Na_2Fe_{1-x}Mn_xPO_4F$ with different proportions of iron and manganese.

2. Experimental

Synthesis of Na_2FePO_4F

A novel sol–gel process was adopted to synthesize Na_2FePO_4F. 0.01 mol iron powder and 0.02 mol citric acid were added to 50 ml deionized water. The ferric citrate solution was obtained under refluxing and stirring conditions at 80 °C for 12 h. Then 0.01 mol $NH_4H_2PO_4$ and 0.02 mol NaF were dissolved in the solution. The obtained mixture was stirred for another 24 h at 80 °C. 0.03 mol ethylene glycol was added to the solution to have a polymerization reaction at 120 °C for 2 h. The gel obtained was dried at 70 °C in a vacuum oven. After thorough grinding, the precursor was pressed into a pellet and calcined in an argon atmosphere at 625 °C for 6 h to get the final product. The redundant fluorine was exhausted by by-products.[13] The carbon content in the composite was determined to be 19.7 wt% (Vario EL III elemental analyzer, Elementar Analysen System GmbH, Germany).

Synthesis of Na_2MnPO_4F

0.01 mol $Mn(NO_3)_2$ solution (50 wt%), 0.02 mol citric acid,0.01 mol H_3PO_4 solution (85 wt%) and 0.02 mol NaF were added to 50 ml deionized water. The mixture was stirred for 24 h at 80 °C. The subsequent steps were exactly the same as that of Na_2FePO_4F. The carbon content was 13.3 wt%.

Synthesis of $Na_2Fe_{1-x}Mn_xPO_4F$

Stoichiometric amounts of iron powder and Mn_2O_3 (total transition metal amount was 0.01 mol), 0.02 mol citric acid and the desired amount of HNO_3 solution were dissolved in 50 ml deionized water and stirred for 12 h at 80 °C. The subsequent steps were the same as that of Na_2FePO_4F. The carbon content of $Na_2Fe_{0.9}Mn_{0.1}PO_4F$, $Na_2Fe_{0.7}Mn_{0.3}PO_4F$ and $Na_2Fe_{0.3}Mn_{0.7}PO_4F$ were 19.4%, 18.4% and 20.6%, respectively.

Characterization

The crystalline phase of the samples was identified by Panalytical X-pert diffractometer (PANalytical, Netherlands) with Cu Kα radiation operated at 40 kV and 30 mA from $2\theta = 10°$ to 70° using a step size of 0.00835 with a counting time of 30 s per step. Rietveld refinement was performed using the GSAS (General Structure Analysis System) program to obtain the crystal structure parameters. Scanning electron microscopy (SEM) studies were performed on S-4800 (HITACHI, Japan), equipped with an energy-dispersive X-ray spectroscopy (EDS) detector used for EDS elemental mapping. The transmission electron microscopy (TEM) and high resolution transmission electron microscopy (HRTEM) were performed on Tecnai F30 (Philips-FEI, Netherlands), operated at an accelerating voltage of 300 kV.

Measurement of electrochemical performances

Electrochemical characterization of the cathode materials was carried out with CR2025 coin-type cells. The cathode was prepared by mixing 70% of the active material with 20% acetylene black and 10% poly(vinylidene fluoride) (PVDF). The mixture was made into a slurry by ball milling using

N-methyl-2-pyrrolidene (NMP) as the solvent. The slurry was then coated onto an Al foil with diameter of 1.6 cm and dried at 120 °C for 1 h. The cells were assembled with the cathode as prepared, with lithium metal as the anode, and with Celgard 2300 as a separator. The electrolyte was 1 M $LiPF_6$ dissolved in ethylene carbonate (EC) and dimethyl carbonate (DMC) (1 : 1 volume ratio). Cells were assembled in argon-filled glove box. Charge/discharge testing was performed galvanostatically between 1.5–4.6 V at a current density of 10 mA g^{-1} at 60 °C (Land CT2001A). The charge/discharge capacities mentioned in this manuscript were calculated based on the mass of $Na_2Fe_{1-x}Mn_xPO_4F$.

3. Results and discussion

The XRD patterns and full pattern refinement of Na_2FePO_4F and Na_2MnO_4F are shown in Fig. 1. All the Bragg peaks could be fully indexed in an orthorhombic structure with space group *Pbcn* and a monoclinic structure with space group $P2_1/n$ for Na_2FePO_4F and Na_2MnPO_4F, respectively. No impurity phases were detected indicating the high phase purity of Na_2FePO_4F and Na_2MnPO_4F samples. The lattice parameters for Na_2FePO_4F refined with GSAS program are a = 5.2316 Å, b = 13.8717 Å, c = 11.7947 Å, and V = 855.956 Å^3. For Na_2MnPO_4F, a = 13.6869 Å, b = 5.3215 Å, c = 13.7155 Å, β = 119.670° and the volume is 867.980 Å^3. The data we obtained above are similar to that reported in ref. 8 and 11.

Fig. 2 shows the crystal structures of Na_2FePO_4F and Na_2MnPO_4F which are two end members of $Na_2Fe_{1-x}Mn_xPO_4F$. As shown in the figure, Na_2FePO_4F has a two-dimensional (2D) layered structure, iron is located in the center of a FeO_4F_2 octahedra coordinated with four oxygen ligands and two fluorine ligands. FeO_4F_2 octahedra shares a O_2F face with another FeO_4F_2 octahedron to form $Fe_2O_6F_3$ bio-ctahedra, which is linked with PO_4 tetrahedra along the c axis direction to form a 2D layered structure. In contrast to Na_2FePO_4F, Na_2MnPO_4F has a three-dimensional (3D) tunnel structure. Manganese is located in the center of a MnO_4F_2 octahedra coordinated with four oxygen ligands and two fluorine ligands. Due to the strong repulsion caused by the large radius of Mn^{2+}, MnO_4F_2 octahedra is corner-shared with another MnO_4F_2 octahedra by fluorine ligand to form $Mn_2O_8F_3$, which shares a corner with PO_4 tetrahedra along the a,c axis direction to form a 3D tunnel structure.

Fig. 3 shows the XRD patterns of $Na_2Fe_{1-x}Mn_xPO_4F$ (x = 0, 0.1, 0.3, 0.7, 1). As seen in the figure, $Na_2Fe_{0.9}Mn_{0.1}PO_4F$ and Na_2FePO_4F have the same structure with the space group of *Pbcn*. But the XRD patterns of samples with greater Mn contents ($x \geq 0.3$) are different. All their Bragg peaks can be indexed as

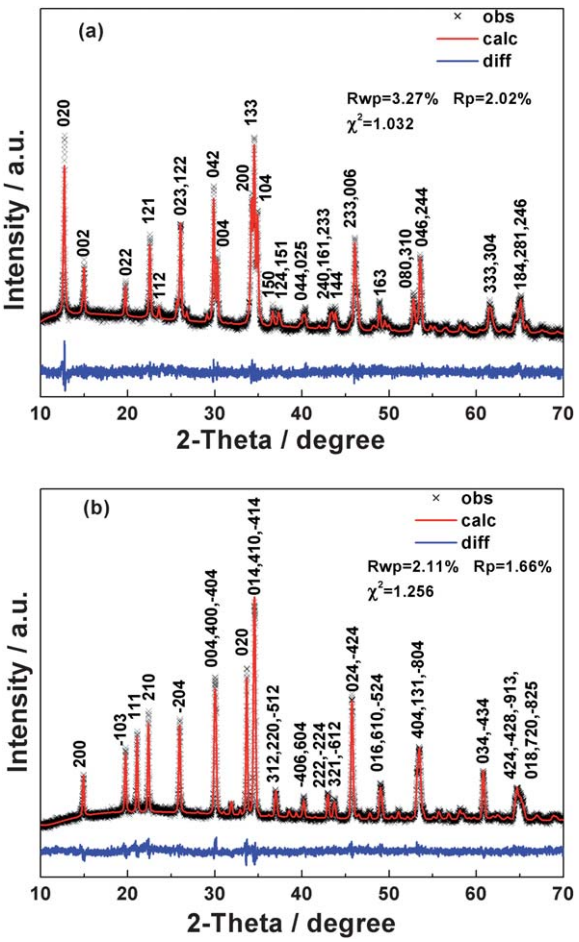

Fig. 1 XRD patterns of (a) Na_2FePO_4F and (b) Na_2MnPO_4F with refined pattern. The experimental data (black cross), calculated patterns (red line), and the difference (blue line) are shown in the figure.

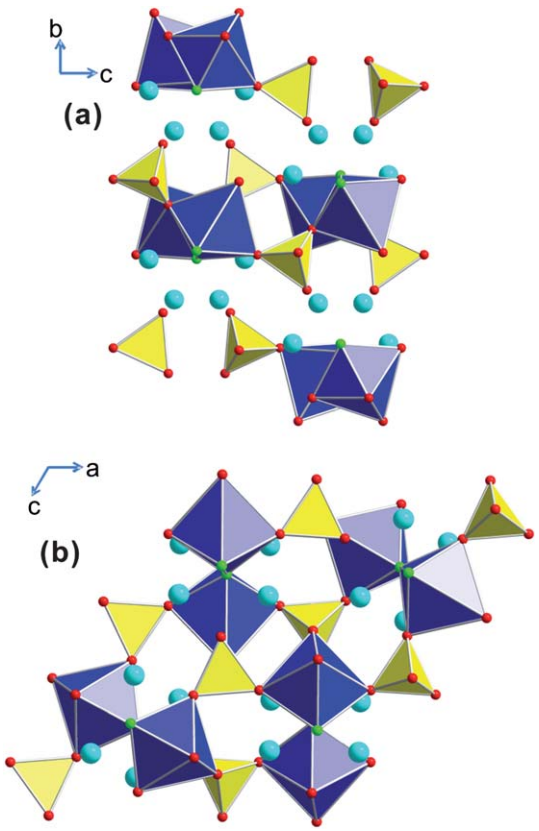

Fig. 2 (a) Crystal structure of Na_2FePO_4F with space group *Pbcn*, viewed along [100], (b) crystal structure of Na_2MnPO_4F with space group $P2_1/n$, viewed along [010].

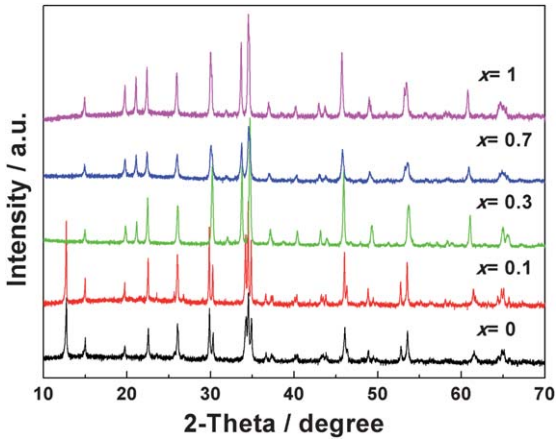

Fig. 3 XRD patterns of $Na_2Fe_{1-x}Mn_xPO_4F$ ($x = 0$, 0.1, 0.3, 0.7, 1).

space group $P2_1/n$ which is the same as Na_2MnPO_4F. This conclusion is consistent with that of Recham's work,[9] which shows that when $x \leq 0.15$, the space group of $Na_2Fe_{1-x}Mn_xPO_4F$ is *Pbcn*, and when x increase to 0.25, the space group changes to $P2_1/n$. They considered that Mn^{2+} has a relatively bigger ionic radius compared with Fe^{2+}, so when it reaches a larger amount, the chance of two MnO_4F_2 octrahedra in adjacent positions increase, which causes stronger repulsive interactions. In order to achieve longer M–M distances so as to minimize the interactions, the structure simply changes to a 3D tunnel corner sharing one. From the XRD patterns of $Na_2Fe_{1-x}Mn_xPO_4F$, we believe that $Na_2Fe_{1-x}Mn_xPO_4F$ solid solution materials were successfully synthesized, although that transition point between two phases is not clear yet. The space group and refined cell parameters of $Na_2Fe_{1-x}Mn_xPO_4F$ ($x = 0$, 0.1, 0.3, 0.7, 1) are summarized in Table 1.

Fig. 4 shows the SEM images of Na_2FePO_4F, Na_2MnPO_4F and $Na_2Fe_{1-x}Mn_xPO_4F$ ($x = 0.1$, 0.3, 0.7). It is clearly seen that the secondary particles of the materials are highly agglomerate and irregular with particle sizes as large as several micrometres. But under high magnification, we can see that the primary particle size is very small, only tens of nanometres. Our TEM experiments also proved our conclusion. Fig. 5 shows the TEM and HRTEM images of Na_2FePO_4F and Na_2MnPO_4F. An amorphous carbon layer covers on the surface of primary particles. A uniform distribution of carbon can be seen and demonstrated from the EDS elemental mappings (Fig. 6), which is also consistent with HRTEM results. This is because Fe^{2+} and Mn^{2+} can be trapped by complexing agents (citric acid and ethylene glycol) to form a homogeneous sol firstly and then, during calcinations, the organic groups decompose to carbon

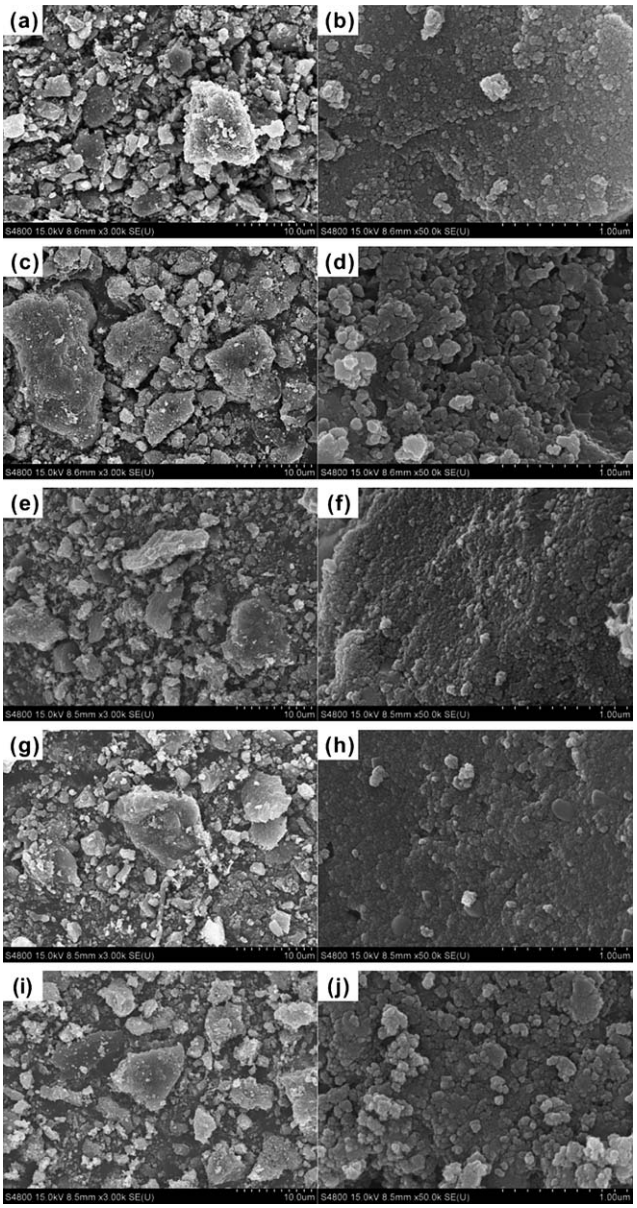

Fig. 4 SEM images of (a, b) Na_2FePO_4F, (c, b) Na_2MnPO_4F, (e, f) $Na_2Fe_{0.9}Mn_{0.1}PO_4F$, (g, h) $Na_2Fe_{0.7}Mn_{0.3}PO_4F$, (i, j) $Na_2Fe_{0.3}Mn_{0.7}PO_4F$.

which can uniformly distribute over each particle and act as a dispersant to form small primary particles. The nanostructure of the material helps to reduce ion diffusion length and uniform carbon distribution helps to increase electronic conductivity of the composite. Thus, the formation of nanostructured carbon

Table 1 Space group and lattice parameters of the $Na_2Fe_{1-x}Mn_xPO_4F$ ($x = 0$, 0.1, 0.3, 0.7, 1)

$Na_2Fe_{1-x}Mn_xPO4F$	Space group	a/Å	b/Å	c/Å	β (°)	V/Å^3
$x = 0$	*Pbcn*	5.2316	13.8717	11.7947	90.00	855.956
$x = 0.1$	*Pbcn*	5.2398	13.8827	11.8022	90.00	858.524
$x = 0.3$	$P2_1/n$	13.6460	5.3056	13.6793	119.753	859.820
$x = 0.7$	$P2_1/n$	13.6646	5.3142	13.6989	119.693	864.592
$x = 1$	$P2_1/n$	13.6869	5.3215	13.7155	119.670	867.980

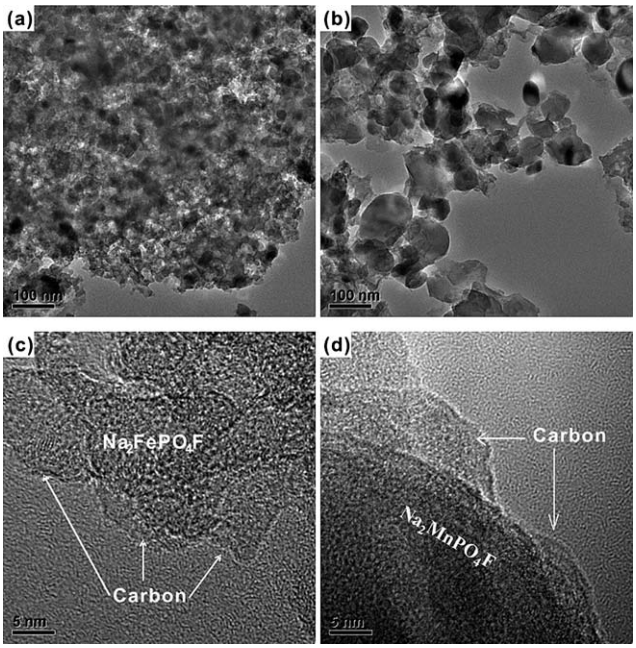

Fig. 5 TEM and HRTEM images of (a, c) Na_2FePO_4F and (b, d) Na_2MnPO_4F.

composite materials is beneficial to enhance electrochemical performance of $Na_2Fe_{1-x}Mn_xPO_4F$. Although solid-state reaction can also achieve a small amount of carbon coating, the materials synthesized have relatively bigger particle sizes.[8,12] In addition, as the ionothermal method may produce small particle size, this method could not realize carbon-coating efficiently.[9] As a consequence, electrochemical performance of materials prepared by the above methods could not be fully utilized.

Fig. 7 shows the charge/discharge profiles of Na_2FePO_4F. The cell based on Na_2FePO_4F had an open circuit voltage (OCV) of 2.93 V, but which slowly dropped to 2.90 V after 24 h equilibration because of Na/Li ion exchange, as also observed by Ellis *et al.*[12] An *ex situ* XRD experiment was also carried out to determine the structural changes of cathode material after equilibrating at OCV for 24 h, the results of which are shown in Fig. 8. It shows that the positions and intensity of the diffraction peaks changed greatly, indicating a structural rearrangement triggered by the ionic exchange of Na^+ and Li^+ in the electrolyte, due to the large difference between ionic radii of Na^+ (102 pm) and Li^+ (76 pm). A high reversible capacity of 182 mA h g^{-1} can be obtained during the first cycle, corresponding to 1.46 electrons exchanged per unit formula. The high reversible capacity with exchange of more than one electron indicates the feasibility of the

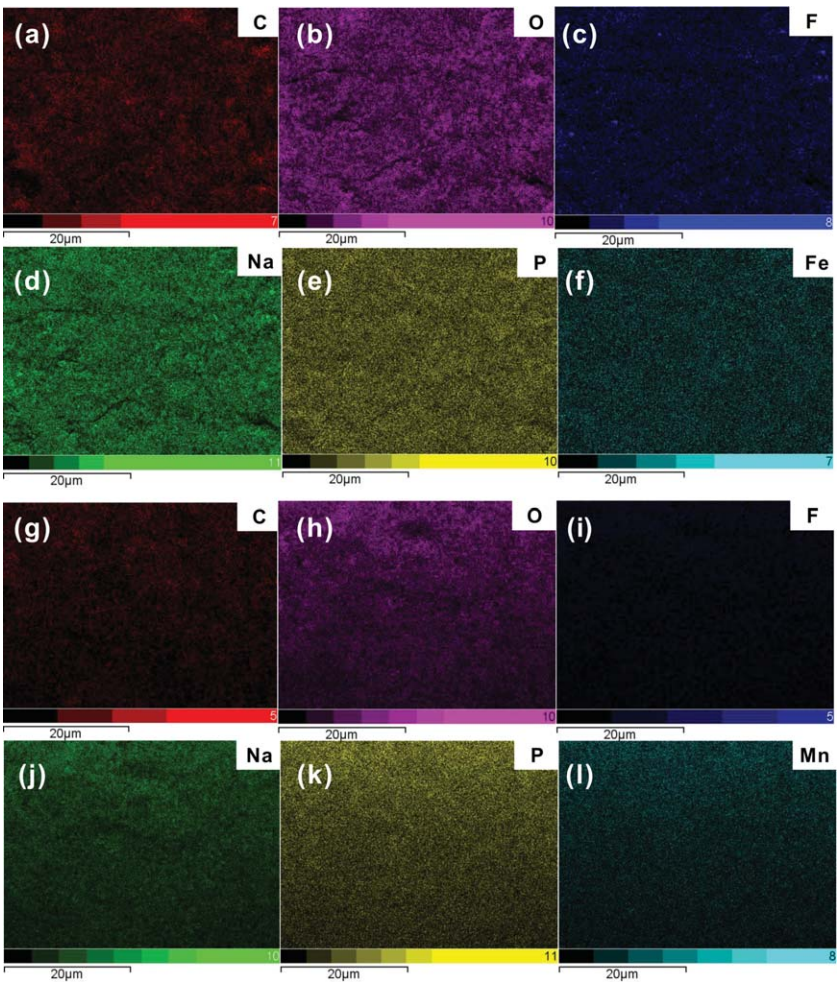

Fig. 6 EDS maps of (a) C, (b) O, (c) F, (d) Na, (e) P, (f) Fe for Na_2FePO_4F and (g) C, (h) O, (i) F, (j) Na, (k) P, (l) Mn for Na_2MnPO_4F.

reversibly extracting/inserting part of the second alkaline ion in Na_2FePO_4F involving the $Fe^{3+/4+}$ couple at high temperature, which has also been reported in Li_2FeSiO_4[14,15] and $LiFePO_4F$[7] materials. During the first charge process, both Li^+ and Na^+ are extracted, but in the following cycles it is most likely that only Li^+ ions are extracted gradually because Li^+ replaces Na^+ in the structure after the first discharging process. In the first charge process, it is more difficult for Na^+ to be extracted because of its larger radius than Li^+, which may result in a bigger overpotential and higher charge voltage. However, since Li^+ ions are inserted into the structure during the first discharge process, that is why the initial and following discharge curves are nearly the same. The charge/discharge profiles are basically identical during the subsequent cycling process, which indicates that the electrode structure remains stable during cycling.

As reported in the literature,[10] Mn-based phosphate materials possess higher redox potential than Fe-based phosphate materials. In order to increase the energy density of Li-ion batteries, Mn-based fluorophosphate cathode material would be a good choice. Ellis *et al.* studied the electrochemical properties of Na_2MnPO_4F prepared by solid-state reaction.[12] However, in their work, Na_2MnPO_4F was found to be electrochemically inactive even when it is charged up to 5 V. This may be due to the bigger primary particle of materials prepared by solid-state method than that prepared by the sol–gel method.[16] Fig. 9 shows the charge/discharge profiles of the obtained nano-Na_2MnPO_4F. The initial discharge capacity of Na_2MnPO_4F is 98 mA h g^{-1} (0.79 electron exchange per unit formula) indicating Na_2MnPO_4F with a three-dimensional (3D) tunnel structure can provide channels for Na^+/Li^+ diffusion and show reasonable electrochemical activity, which is consistent with Recham's results that the 3D tunnel structure of $Na_2Fe_{1-x}Mn_xPO_4F$ ($x \geq 0.25$) with the same structure of Na_2MnPO_4F has alkali ion diffusion pathways.[9] These results indicated that the electrochemical inactivity of Na_2MnPO_4F observed previously by Ellis *et al.* and Recham *et al.* is mainly due to the bigger particle size with or without carbon coating rather than the structural distinction of Na_2MnPO_4F.[9,12] The Na_2MnPO_4F material prepared by our novel sol–gel method has small primary particles and uniform carbon distribution, which greatly enhance the electronic conductivity of the material. Meanwhile charge/discharge at an elevated temperature of 60 °C also helps to enhance electrode kinetics.[15] Unfortunately, no more than one electron exchange or higher voltage plateau than that of Na_2FePO_4F can be achieved yet. This probably due to the relatively poor electrochemical activity of Mn-based materials compared with Fe-based ones,[17] resulting in Mn-based fluorophosphates showing high polarization and low discharge voltage plateau. Meanwhile, Na_2MnPO_4F also suffers unsatisfactory cycling stability with only 47% capacity retention after 20 cycles. Efforts are underway to study its fading mechanism.

Fig. 10 shows the initial charge/discharge profiles of $Na_2Fe_{1-x}Mn_xPO_4F$ ($x = 0$, 0.1, 0.3, 0.7, 1) cathode materials. The voltage plateau of discharge curves becomes higher with the increase of Mn content, especially when $x = 0.7$; an obvious discharge plateau can be seen at ~4 V, corresponding to reversible reaction with the $Mn^{2+/3+}$ redox couple. It is speculated that it is due to Mn having a relatively higher redox voltage. Thus, the substitution of Fe for Mn in $Na_2Fe_{1-x}Mn_xPO_4F$ can increase the discharge potential (*i.e.* energy density) of the material. In our results, $Na_2Fe_{1-x}Mn_xPO_4F$ ($x = 0.1$, 0.3, 0.7) electrodes deliver discharge capacities of 169 mA h g^{-1}, 176 mA h g^{-1} and 169 mA h g^{-1}, corresponding to 1.35, 1.42 and 1.36 electrons exchanged per unit formula, respectively. Good electrochemical performance can still be observed for materials with Mn content up to 0.7. The improved electrochemical performance of $Na_2Fe_{1-x}Mn_xPO_4F$ ($x = 0$, 0.1, 0.3, 0.7, 1) compared with that obtained by solid-state reaction or ionothermal process could be, at least in part, attributed to the nanoparticle distribution and improved electronic conductivity *via* nanostructured carbon composite. From these results, it is found that the increase of the amount of manganese in $Na_2Fe_{1-x}Mn_xPO_4F$ results in an increase of the discharge plateau, but accompanied by a slight decrease of discharge capacity. A 4 V plateau appears with the introduction of manganese and becomes more obvious when x is further increased. However, Mn-based materials suffer from poor

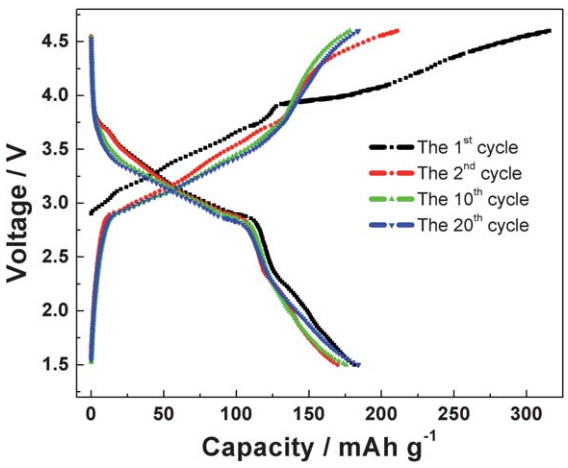

Fig. 7 Charge/discharge profiles of Na_2FePO_4F cathode material over the voltage range of 1.5–4.6 V at a current density of 10 mA g^{-1} at 60 °C.

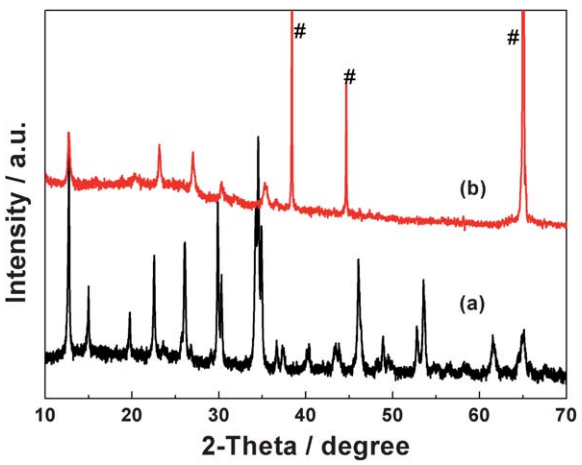

Fig. 8 XRD patterns of (a) Na_2FePO_4F and (b) the cathode assembled from the cell based on Na_2FePO_4F equilibrated for 24 h at open circuit voltage (OCV). The XRD peaks corresponding to current collector Al is represented by the symbols #.

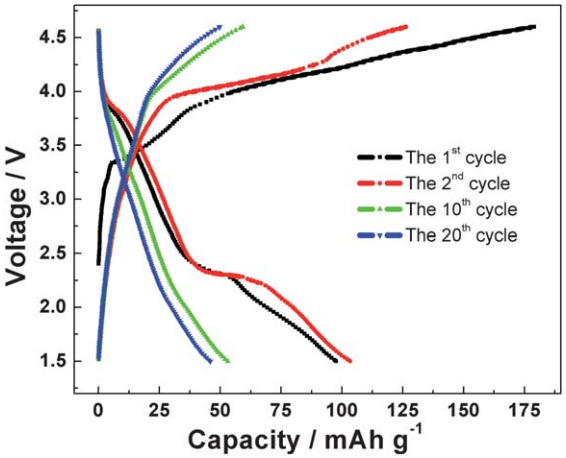

Fig. 9 Charge/discharge profiles of Na_2MnPO_4F cathode material over the voltage range of 1.5–4.6 V at a current density of 10 mA g^{-1} at 60 °C.

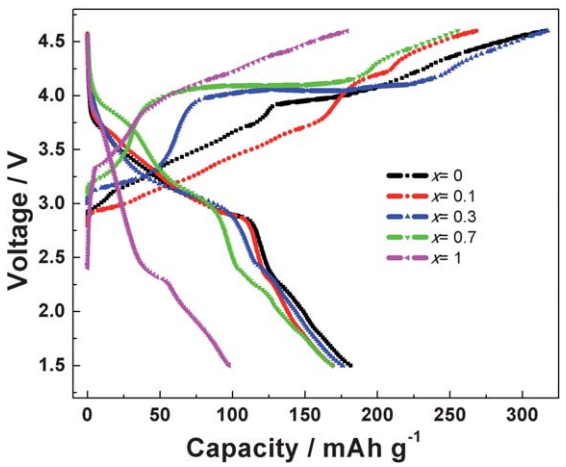

Fig. 10 The initial charge/discharge profiles of $Na_2Fe_{1-x}Mn_xPO_4F$ (x = 0, 0.1, 0.3, 0.7, 1) cathode materials over the voltage range of 1.5–4.6 V at a current density of 10 mA g^{-1} at 60 °C.

electrochemical activity, so introduction of manganese also increases kinetic polarization which results in decreasing discharge capacity. Especially, when x increases from 0 to 1, Fe free material such as Na_2MnPO_4F delivers worse discharge capacity and shows no obvious discharge plateau. The addition of Fe to Mn-based materials can improve their electrochemical activity, which has been confirmed by $LiMn_yFe_{1-y}PO_4$ materials.[18,19] So the proper ratio of iron and manganese in $Na_2Fe_{1-x}Mn_xPO_4F$ may achieve excellent electrochemical performance.

The cycling performances of $Na_2Fe_{1-x}Mn_xPO_4F$ (x = 0, 0.1, 0.3, 0.7, 1) are also shown in Fig. 11. Na_2FePO_4F and Mn-substituted fluorophosphates $Na_2Fe_{1-x}Mn_xPO_4F$(x = 0.1, 0.3, 0.7) all exhibit good cycling stability when tested at high temperature of 60 °C. The result is quite different from that reported for $Li_2Fe_{1-x}Mn_xSiO_4$.[20] The substitution of Fe by Mn damages the cycling stability, probably due to Jahn–Teller distortion of Mn^{3+}. The $Na_2Fe_{1-x}Mn_xPO_4F$ (x = 0, 0.1, 0.3, 0.7) materials as-prepared can deliver more than one electron in the charge/discharge process. However, in Mn-doped

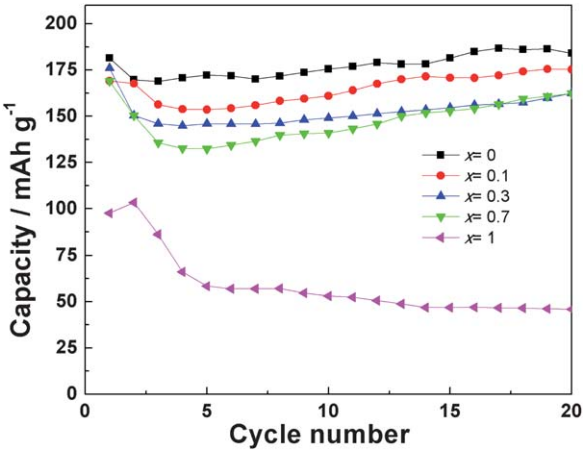

Fig. 11 Lifecycle performance of $Na_2Fe_{1-x}Mn_xPO_4F$ (x = 0, 0.1, 0.3, 0.7, 1) cathode materials over the voltage range of 1.5–4.6 V at a current density of 10 mA g^{-1} at 60 °C.

materials $Na_2Fe_{1-x}Mn_xPO_4F$, whether Fe or Mn contributes most to the capacity and capacity-retention result needs further systematic study, *e.g. in situ* XAS (X-ray absorption spectroscopy) study.

4. Conclusions

Nanostructured fluorophosphates such as $Na_2Fe_{1-x}Mn_xPO_4F/C$ (x = 0, 0.1, 0.3, 0.7, 1) composite cathode materials were successfully prepared by a novel sol–gel process. It is shown that Na_2FePO_4F and $Na_2Fe_{0.9}Mn_{0.1}PO_4F$ have the same structure with space group *Pbcn*. However, $Na_2Fe_{0.7}Mn_{0.3}PO_4F$ and $Na_2Fe_{0.3}Mn_{0.7}PO_4F$ have the same structure as that of Na_2MnPO_4F in space group $P2_1/n$. The small primary particle formed in the as-prepared materials mainly due to the relatively low synthesis temperature and uniform carbon distribution inhibiting particle growth and aggregation. When cycled at 60 °C, Na_2FePO_4F material exhibits an initial discharge capacity of 182 mA h g^{-1} (corresponding to 1.46 electrons exchanged per unit formula) with good cycling stability. This indicates that the $Fe^{3+/4+}$ redox couple could be accessible for nano-Na_2FePO_4F prepared by the novel sol–gel method. The electrochemical activity of Na_2MnPO_4F can be achieved *via* decreasing particle size and uniform carbon distribution, with an initial discharge capacity of 98 mA h g^{-1}. Similar to results observed in olivine phosphates and orthosilicates, pure manganese based material Na_2MnPO_4F shows poorer electrochemical performance compared with its iron counterpart Na_2FePO_4F. The charge/discharge potential of $Na_2Fe_{1-x}Mn_xPO_4F$ increases with Mn content. A distinct plateau at ~4 V can be obviously observed for $Na_2Fe_{0.3}Mn_{0.7}PO_4F$. The lithiation/delithiation plateau located at ~4 V indicates the occurrence of reversible reaction with $Mn^{2+/3+}$ redox couple.

Acknowledgements

We are grateful for the financial support of the research reported in this paper: National Basic Research Program of China (973 program, Grant No. 2011CB935903 and 2007CB209702) and the

National Natural Science Foundation of China (Grant No. 20873115, 21021002 and 90606015, *etc.*).

References

1 J. M. Tarascon, *Philos. Trans. R. Soc. London, Ser. A*, 2010, **368**, 3227.
2 A. K. Padhi, K. S. Nanjundaswamy and J. B. Goodenough, *J. Electrochem. Soc.*, 1997, **144**, 1188.
3 Q. M. Zhang, Z. C. Shi, Y. X. Li, D. Gao, G. H. Chen and Y. Yang, *Acta Phys. -Chim. Sin.*, 2011, **27**, 267.
4 Z. Gong and Y. Yang, *Energy Environ. Sci.*, 2011, **4**, 3223.
5 J. Barker, M. Y. Saidi and J. L. Swoyer, *J. Electrochem. Soc.*, 2003, **150**, A1394.
6 T. N. Ramesh, K. T. Lee, B. L. Ellis and L. F. Nazar, *Electrochem. Solid-State Lett.*, 2010, **13**, A43.
7 N. Recham, J. N. Chotard, J. C. Jumas, L. Laffont, M. Armand and J. M. Tarascon, *Chem. Mater.*, 2010, **22**, 1142.
8 B. L. Ellis, W. R. M. Makahnouk, Y. Makimura, K. Toghill and L. F. Nazar, *Nat. Mater.*, 2007, **6**, 749.
9 N. Recham, J. N. Chotard, L. Dupont, K. Djellab, M. Armand and J. M. Tarascon, *J. Electrochem. Soc.*, 2009, **156**, A993.
10 J. Molenda, W. Qjczyk and J. Marzec, *J. Power Sources*, 2007, **174**, 689.
11 O. V. Yakubovich, O. V. Karimova and O. K. Melnikov, *Acta Crystallogr., Sect. C: Cryst. Struct. Commun.*, 1997, **53**, 395.
12 B. L. Ellis, W. R. M. Makahnouk, W. N. Rowan-Weetaluktuk, D. H. Ryan and L. F. Nazar, *Chem. Mater.*, 2010, **22**, 1059.
13 D. Y. Wang, J. Xiao, W. Xu, Z. M. Nie, C. M. Wang, G. Graff and J. G. Zhang, *J. Power Sources*, 2011, **196**, 2241.
14 D. Lv, W. Wen, X. Huang, J. Bai, J. Mi, S. Wu and Y. Yang, *J. Mater. Chem.*, 2011, **21**, 9506.
15 T. Muraliganth, K. R. Stroukoff and A. Manthiram, *Chem. Mater.*, 2010, **22**, 5754.
16 J. M. Zheng, X. B. Wu and Y. Yang, *Electrochim. Acta*, 2011, **56**, 3071.
17 R. Dominko, C. Sirisopanaporn, C. Masquelier, D. Hanzel, I. Arcon and M. Gaberscek, *J. Electrochem. Soc.*, 2010, **157**, A1309.
18 T. Muraliganth and A. Manthiram, *J. Phys. Chem. C*, 2010, **114**, 15530.
19 A. Yamada and S. C. Chung, *J. Electrochem. Soc.*, 2001, **148**, A960.
20 Z. L. Gong, Y. X. Li and Y. Yang, *Electrochem. Solid-State Lett.*, 2006, **9**, A542.